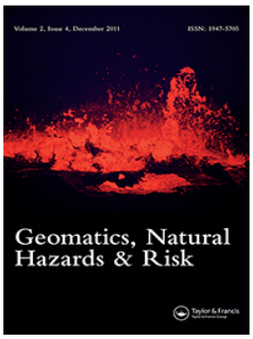

Geomatics, Natural Hazards and Risk

ISSN: 1947-5705 (Print) 1947-5713 (Online) Journal homepage: www.tandfonline.com/journals/tgnh20

A novel per pixel and object-based ensemble approach for flood susceptibility mapping

Thimmaiah Gudiyangada Nachappa & Sansar Raj Meena

To cite this article: Thimmaiah Gudiyangada Nachappa & Sansar Raj Meena (2020) A novel per pixel and object-based ensemble approach for flood susceptibility mapping, Geomatics, Natural Hazards and Risk, 11:1, 2147-2175, DOI: 10.1080/19475705.2020.1833990

To link to this article: https://doi.org/10.1080/19475705.2020.1833990

Published online: 14 Oct 2020.

GEOMATICS, NATURAL HAZARDS AND RISK
2020, VOL. 11, NO. 1, 2147–2175
https://doi.org/10.1080/19475705.2020.1833990

Taylor & Francis
Taylor & Francis Group

A novel per pixel and object-based ensemble approach for flood susceptibility mapping

Thimmaiah Gudiyangada Nachappa and Sansar Raj Meena

Department of Geoinformatics–Z_GIS, University of Salzburg, Salzburg, Austria

ABSTRACT

Conducting flood susceptibility assessments is critical for the identification of flood hazard zones and the mitigation of the detrimental impacts of floods in the future through improved flood management measures. The significance of this study is that we create ensemble methods using the per-pixel approaches of frequency ratio (FR), analytical hierarchical process (AHP), and evidence belief function (EBF) used for weightings with the object-based 'geons' approach used for aggregation to create a flood susceptibility map for the East Rapti Basin in Nepal. We selected eight flood conditioning factors considered to be relevant in the study area. The flood inventory data for the East Rapti basin was derived from past flood inventory datasets held in the regional database system by the International Centre for Integrated Mountain Development (ICIMOD). The flood inventory was classified into training and validation datasets based on the widely used split ratio of 70/30. The Receiver Operating Characteristic (ROC) was used to determine the accuracy of the flood susceptibility maps. The AUC results indicated that the combined per-pixel and object-based geon approaches yielded better results than the per-pixel approaches alone. Our results showed that the object-based geon approach creates meaningful regional units that are beneficial for future planning.

ARTICLE HISTORY
Received 6 July 2020
Accepted 30 September 2020

KEYWORDS
Floods; flood susceptibility; object-based image analysis; FR; AHP; EBF; natural hazards

1. Introduction

Water is crucial for sustaining life, but it has become a significant focus in recent years in terms of inadequacy, disaster, and famine. During the past couple of years, the frequency of natural hazards has significantly increased. This can be attributed to increases in precipitation, deforestation, population and infrastructural growth (Pradhan 2009). Floods are the most frequent and expensive natural hazard in terms of loss of human lives and economic resources. Flooding is a recurring, severe, prevalent and accumulative natural hazard occurring around the world (Levy et al. 2007). Most of the time, flooding is caused by frequent and prolonged rainfall within a short duration of time. Flooding appears to be occurring regularly, and there are several

CONTACT Sansar Raj Meena sansaraj.meena@sbg.ac.at

factors that could be influencing and contributing to the flooding. These include an increase in ecological degradation caused by population growth, deforestation, and urbanization along with physiographical factors like the topography, geomorphology and climate (Khosravi et al. 2019). Flooding becomes a disaster when it affects infrastructure, settlements, and people. The intensity and frequency of flooding determine the potential damage and associated losses. Globally, flooding has increased by 40% in the past couple of decades (Hirabayashi et al. 2013). Flooding causes severe damage to various facets of life on earth, including human lives, economy, infrastructure, transportation, and ecological ecosystems (Yu et al. 2013). Flooding can have severe effects on the socio-economic condition of the region in which it occurs. Investigation and analysis of flooding are essential for planning and taking socio-economic and environmental measures (Markantonis et al. 2013). A susceptibility analysis of any natural hazard is essential to be able to forecast the future occurrence of the natural hazard. Flood susceptibility mapping is a prerequisite for management strategies aiming to mitigate the adverse effects of floods (Sachdeva et al. 2017). The communities and infrastructure closest to the rivers are exposed to the direct impacts of flooding and are, therefore, the most vulnerable (Jung et al. 2011).

Advances in technologies like remote sensing (RS), earth observation (EO) and geographic information systems (GIS) have significantly contributed to mitigation and planning measures for future hazards (Ghorbanzadeh et al. 2018a, 2019). In recent years, RS and GIS have been extensively used to evaluate natural hazards (Van Westen et al. 2003; Oh and Pradhan 2011; Meena and Tavakkoli Piralilou 2019). RS, along with GIS, has been used in many studies to analyze flood susceptibility (Rahmati et al. 2015a; Tehrany et al. 2015a; Arabameri et al. 2019; Tien Bui et al. 2019). Natural hazards like floods, landslides, wildfires and earthquakes have been studied using several data-driven and knowledge-based models like Frequency Ratio (FR) (Lee and Pradhan 2007; Rahmati et al. 2015a; Khosravi et al. 2016), Analytical Hierarchical Process (AHP) (Rahmati et al. 2015b; Haghizadeh et al. 2017; Meena et al. 2019a), Evidence Belief Function (EBF) (Althuwaynee et al. 2012; Nampak et al. 2014). Machine learning approaches, such as Support Vector Machines (SVM) (Tehrany et al. 2015a, 2015b), Random Forest (RF) (Chapi et al. 2017; Haghizadeh et al. 2017), Dempster-Shafer (Mohammady et al. 2012; Pourghasemi et al. 2013), Decision Tree (Tehrany et al. 2013), Logistic Regression (LR) (Pradhan et al. 2008; Felicísimo et al. 2013), and Artificial Neural Networks (ANN) (Conforti et al. 2014; Haghizadeh et al. 2017) are also being widely used for susceptibility modelling. The FR is a data-driven approach based on past flooding events, the causative factors and the spatial coverage of the flooding (Wu et al. 2016). Several studies have used FR to generate flood susceptibility maps (Samanta et al. 2018; Arabameri et al. 2019). Object-based image analysis (OBIA) has become a crucial part of GIScience dedicated to the assessment and analysis of satellite imagery (Hay and Castilla 2008). OBIA is used to carry out image analysis, which involves image segmentation and image classification. In a recent study, the machine learning techniques naïve Bayes and naïve Bayes tree were compared with the multi-criteria decision technique, Technique of Order Preference Similarity to the Ideal Solution (TOPSIS). This study showed that machine learning (ML) has a higher prediction power compared to expert-based

multi-criteria decision analysis (MCDA) (Khosravi et al. 2019). The evidence belief function (EBF) and ensemble techniques have also been applied for flood susceptibility analysis and compared with technique for order preference by similarity to an ideal solution (TOPSIS), classification and regression trees (CART), vlseKriterijumska optimizacija I kompromisno resenje (VIKOR) and FR techniques, and it was determined that the EBF model yielded a higher accuracy (Mosavi et al. 2018; Arabameri et al. 2019; Chowdhuri et al. 2020). Advanced ML methods, like feature selection (simulate annealing) with resampling algorithms, have also been used for flood susceptibility mapping (Hosseini et al. 2020). ML and other statistical approaches have been widely used in other natural hazard assessments like landslide, earthquake, wildfire, and gully erosion studies. The random subspace-based classification and regression tree (RSCART) along with CART and logistic regression to benchmark the models (Li and Chen 2019) has also been used for landslide susceptibility mapping, as has the EBF model along with logistic regression and logistic model tree (Zhao and Chen 2020). RF, Credal decision trees, kernel logistic regression and best-fit decision trees have been used for gully erosion susceptibility analysis (Lei et al. 2020a). A series of tree-based ensemble methods have been used for groundwater spring potential mapping to estimate the efficiency and predictive ability (Chen et al. 2020b). All these ML and MCDA methods are powerful; however, they are also sensitive to some issues and exhibit certain weaknesses or uncertainties. In the case of ML methods, as the models are trained, they are prone to overlearning, and the selection of the number of epochs in the training process may influence the results. Furthermore, the input data used for ML are typically specified to take a wide range of values, while their output results are within limited ranges.

The object-based classification presents a feasible alternative for the pixel-based approach (Benz et al. 2004). The image segmentation process is a crucial prerequisite for classification (Blaschke et al. 2014) and further analysis in the geon method. According to Lang et al. 'Geons are spatial units that are homogenous in terms of varying space and time phenomena under policy concern' (Lang et al. 2014). The geon approach integrates expert knowledge and semi-automatically delineates regions. Any suitable model can be used for the assessment of natural hazards, and every model has benefits and drawbacks over other models. The performance of each model depends on the type of data used, the level of accuracy, and the structure. There is also no indication that a specific model should be used for a particular scenario or study area (Khosravi et al. 2018).

The East Rapti Basin is situated in the central Nepalese development region. Over the years, several natural hazards, like floods and landslides, have occurred in the study area and affected the lives of thousands of people. Flooding occurs quite frequently during the annual monsoon season due to heavy precipitation throughout Nepal.

Nepal is one of the world's countries most affected by natural hazards such as floods (Kargel 2016). Extreme rainfall events during the monsoon season cause regular flooding in Nepal almost every year. In the low-lying areas of Nepal (Trai region), riverine flooding and inundation are key hazards. Due to climate change and the prevalent topography in the east Rapti basin, flooding occurs almost every year.

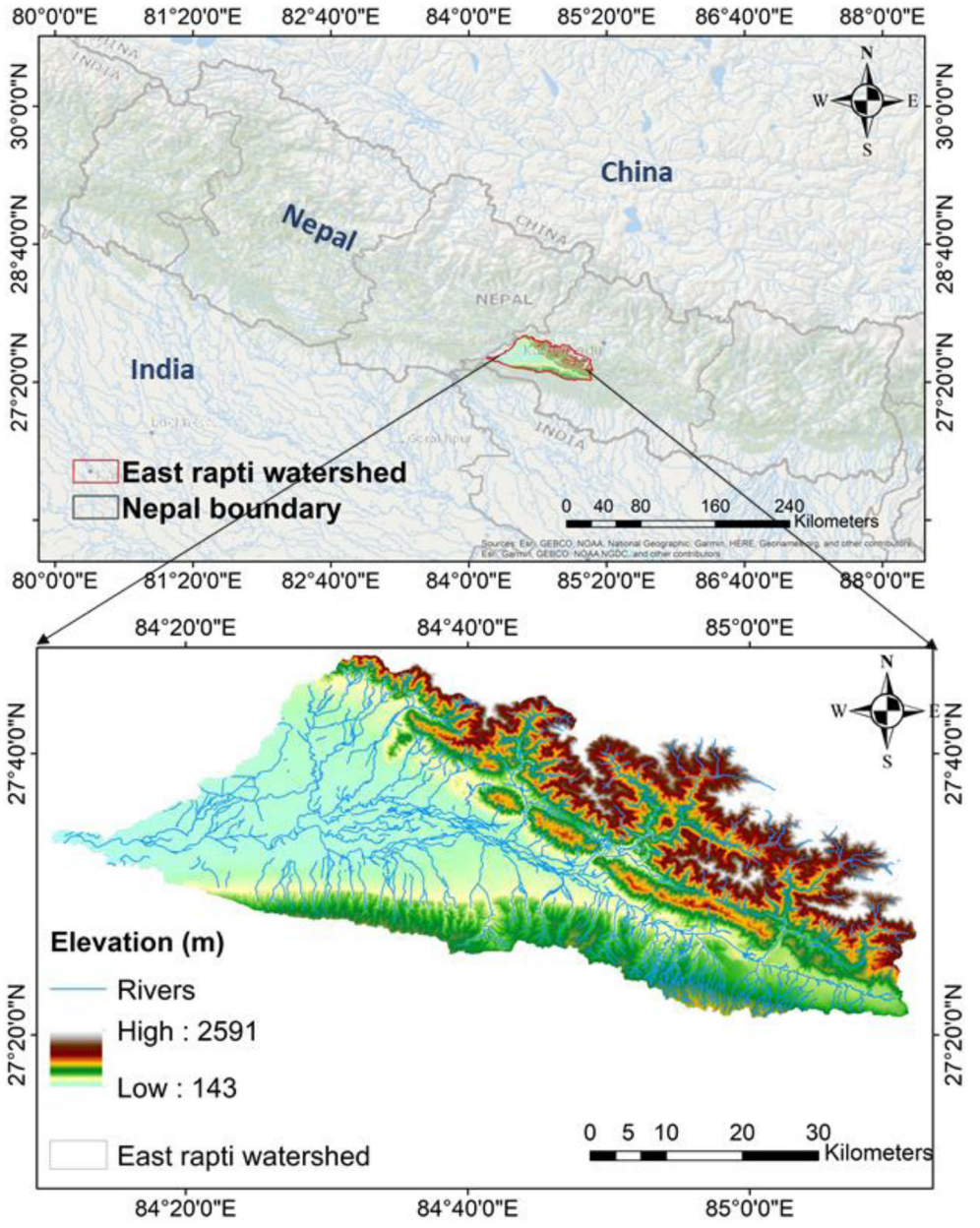

Figure 1. Figure shows the study area along with the elevation map of the region.

Apart from the topography and climate change, several other factors such as deforestation, increased unplanned urban growth, blocked drainage systems, and poor planning contribute to flooding in the area.

The main goal of this study is to compare the results of traditional, simple to use per-pixel methodologies like FR, AHP and EBF for flood susceptibility mapping with the ensemble of per-pixel (weighting) and object-based (aggregation) approach of geons. These assessments would enable us to ascertain which approach is the most suitable for flood susceptibility mapping in the East Rapti Basin in Nepal. The main advantage of the

geon approach is that it can be applied in regions that are devoid of administrative boundaries. This research provides a detailed analysis of whether the object-based geons approach yields better results than the traditional per-pixel approaches.

2. Study area

The East Rapti Basin is in the central development region of Nepal, which is located in the southern part of central Nepal (See Figure 1). The total basin area is 2537 km^2 and covers about 58% of the area of Chitwan district.

The source of the East Rapti River lies in the southern part of the lesser Himalayas about 25 kilometres southwest of Kathmandu. The course of the river is 122 km long. It flows towards the west where it joins the larger glacial river Narayani. The East Rapti river flows for about 122 km, winding through alluvial deposits and gathering tributaries from the northern part along its course. There is a sharp gradient in elevation between the origin of the river at 1500 m and the exit point of the river from the basin at 140 m. Due to this gradient, the river basin has a very diverse biophysical environment. The river flows from the mountains to the valleys of the Churia and Shiwalik hills covering the valley floor of the Chitwan and Makwanpur district. The valley of Chitwan is a tectonic depression buried beneath the alluvial deposits. The mountain terrain of the basin has slopes of between less than 10° and 30°. A large part of the middle Himalayan mountains has a proper drainage system; the drainage system in Siwalik is hugely inconsistent because of varied topography and is prone to flooding close to the river Rapti. The East Rapti river serves as a significant source of livelihoods for the people in settlements distributed throughout the Makwanpur district situated upstream, and the Chitwan valley situated downstream of the valley. The East Rapti River has already faced substantial floods, which the many tributaries beginning in the mountains contributed to. In the upstream region, soil erosions and landslides are prominent, whereas floods and debris flow are more prevalent downstream.

3. Data and methods

3.1. Flood inventory

The flood inventory data were derived from a past flood inventory dataset held in the regional database system by the International Centre for Integrated Mountain Development (ICIMOD). There are 1719 flood locations in the flood inventory dataset that we used for the flood susceptibility mapping of the East Rapti basin. There is no standard process for the selection of training and testing data, and we chose the most commonly used 70/30 ratio for creating training and validation subsets from the flood data. The training data (70%) comprises 1207 flood location points, and the validation data (30%) encompasses 512 flood location points in the East Rapti basin.

3.2. Flood conditioning factors

The conditioning factors are crucial for any susceptibility analysis. The flood conditioning factors were chosen based on the study area, literature studies, data

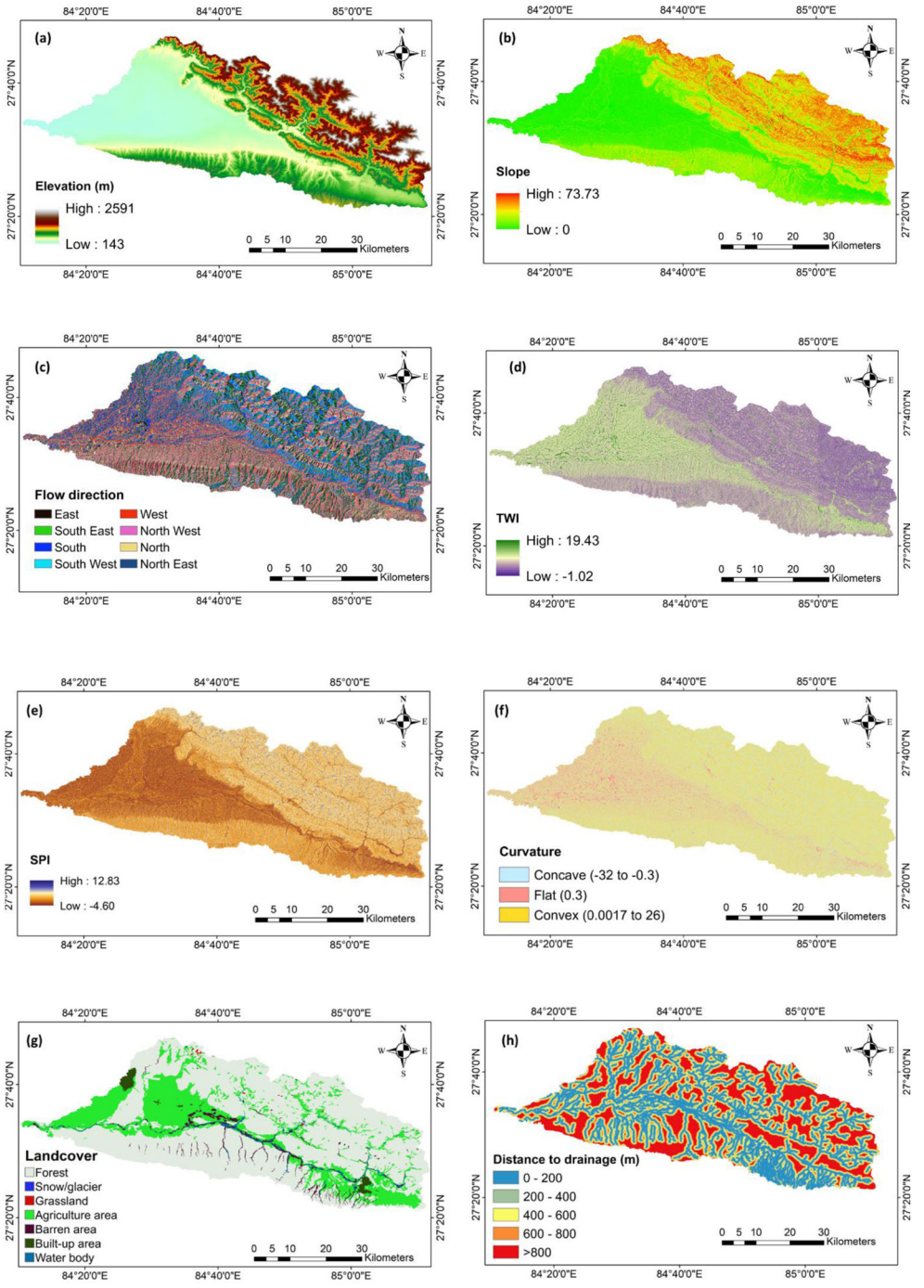

Figure 2. The flood conditioning factors used for the East Rapti Basin in Nepal.

availability, and feedback from the expert for the East Rapti basin in Nepal. We used eight conditioning factors for the study area, namely elevation, curvature, slope, distance from drainage, landcover, TWI, SPI and flow direction. A Shuttle Radar

Topography Mission (SRTM) DEM from national aeronautics and spatial administration (NASA) with a resolution of 30 m was used to derive the input conditioning factors of elevation, slope, curvature, TWI, SPI, flow direction and distance from drainage. The 30 m resolution DEM is a global 1-arcsecond that is publicly available through the United States Geological Survey's Earth Explorer site (http://earthexplorer.usgs.gov/). The landcover data was obtained from the Regional database system from the International Centre for Integrated Mountain Development (ICIMOD). All the conditioning factors shown in Figure 2 were reclassified to 30 m cell size resolution for consistency and, ultimately, to carry out the flood susceptibility analysis. There is no acknowledged standard for the classification of conditioning factors (Kumar and Anbalagan 2016). The nature of the study area, the relevance of each factor for the study area, and the information available within the dataset were taken into consideration when the conditioning factors were classified.

The elevation is an essential factor in flood susceptibility analysis (Rahmati et al. 2015b). Elevation can influence topographic factors and vegetation distribution (Khosravi et al. 2016). The elevation layer was categorized into the following five classes: 0–400 m,400–800 m, 800–1200 m, 1200–1600 m and >1600 m.

The slope is crucial in flood susceptibility analysis as it regulates the surface runoff velocity and vertical filtration, which affects the flood susceptibility. The slope is measured as the surface indicator for flood susceptibility (Youssef et al. 2011). The slope was classified into the following five classes: 0°–5°, 05°–12°, 12°–20°, 20°–28° and >28°.

The curvature can be used to extract valuable geomorphological information (Tehrany et al. 2015a). In plan curvature, concave shows a negative curvature, flat is represented by flat curvature, and convex shows a positive curvature. The curvature was classified into the three classes of concave, flat and convex.

The topographical wetness index (TWI) is the accumulation of flow at any given locality in the catchment with the attention of downstream flow tendencies due to the gravity (Gokceoglu et al. 2005). Equation (1) was used to calculate the TWI (Beven and Kirkby 1979; Moore et al. 1991) is

$$TWI = ln(\alpha / \tan \beta) \tag{1}$$

(Beven and Kirkby 1979; Moore et al. 1991)

Where α is the cumulative upslope area draining through a point (per unit contour length) and tan β is the slope angle in degrees at that given point. The TWI was classified into the following five classes: <8, 8–10, 10–12, 12–14 and >14.

The stream power index (SPI) is the influence of water flow on erosion. Equation (2) was used to calculate the SPI, as is given by (Moore et al. 1991)

$$SPI = (\alpha \ X \ \tan \beta) \tag{2}$$

(Moore et al. 1991)

Where α is the specific area of the catchment in m^2/m of the catchment, and tan β is the slope angle in degrees at that point. The SPI was classified into the following 5 classes: <–2, –2–0.22, 0.22–1.55, 1.55–4.15 and >4.15.

The region encompasses highly diverse landcover zones (Mohammadi et al. 2019). Landcover maps were sourced from the International Centre for Integrated Mountain Development (ICIMOD) (SERVIR Himalaya project). For land cover mapping, Landsat TM satellite images of 30 m spatial resolution were used from 2009, 2010 and 2011. The GEOBIA classification technique was adopted for Landsat TM satellite image classification. At least 10 reference segments were selected for each class using field data and very high resolution satellite imagery to develop the rules (Uddin et al. 2015)

Land use is one of the vital conditioning factors for flood susceptibility assessments. The landcover is classified into the following seven classes: forest, snow/glacier, grassland, agricultural area, barren land, built-up area, and waterbody.

Distance from drainage is the leading influencing factor in flood susceptibility and has a substantial impact on the coverage and magnitude of the flooding (Glenn et al. 2012). The study area was categorized into the following five classes: 0–400 m, 400–800 m, 800–1200 m, 1200–1600 m, and >1600 m.

Flow direction was classified into the following eight classes: east, south-east, south, southwest, west, north-west, north and northeast.

3.3. Methodology

The flood susceptibility analysis was carried out using the simple traditional per-pixel approaches of data-based frequency ratio (FR), expert-based analytical hierarchical process (AHP), and evidence belief function (EBF). The results of these analyses were then compared to the per-pixel and object-based ensemble approach of geons with FR, AHP and EBF. There are various approaches for flood susceptibility mapping, and the main reason for choosing the per-pixel based approaches and the per-pixel and object-based ensemble approach was to understand the impact of aggregation using the object-based approach. We used geons, an object-based aggregation approach, where the weights are derived from the per-pixel approaches for aggregation to produce flood susceptibility maps that are devoid of administrative boundaries (See Figure 3).

3.3.1. Frequency ratio (FR)

The FR model is generally applied in the field of natural hazard susceptibility analysis. FR is a simple assessment method used to determine the probability of the occurrence and non-occurrence of floods for every factor chosen for specific study area (Lee and Pradhan 2007; Wang and Li 2017). FR is a variant of the probabilistic model based on the detected relationships between the flood distribution and the related factors of flooding (Lea Tien Tay et al. 2014), and thus shows the correlation between flooding locations and the influencing factors inducing the floods that have occurred in the given area.

The flood conditioning factors can be weighted by considering the ratio of observed floods to the area of the selected study area. The correlation between factor classes can be found through the FR, which is a useful geospatial assessment tool (Mahalingam et al. 2016; Meena and Gudiyangada Nachappa 2019; Meena et al. 2019b). The FR weights are computed through the ratio of flood inventory locations for all classes within each factor. The flood inventory points are blanketed with the

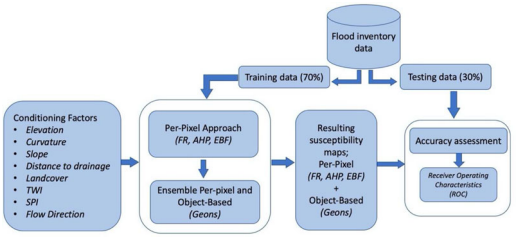

Figure 3. The overall workflow and methodology for the East Rapti basin.

conditioning factors to acquire the ratio of the area of each factor class to the total area. The FR weights are then obtained by dividing the flood occurrence ratio by the area in that class (Demir et al. 2013). The FR methodology uses the weighted sum approach to produce the final susceptibility map. The flood susceptibility index (FSI) is computed through the summation of the individual conditioning factor ratio values resulting from the FR calculation given in Equation (3) below (Lee and Pradhan 2007).

$$\mathrm{FSI} = \sum \mathrm{FR} \tag{3}$$

$$FSI = (elevation{*}wi) + (slope * wi) + (curvature * wi) + (twi * wi) + (spi * wi) + (landcover * wi) + (distance\ to\ streams * wi) + (flow\ direction * wi) \tag{4}$$

Where FSI is the flood susceptibility index, FR is the frequency ratio of every factor type or class, and *wi* is the weight of each conditioning factor. The higher the FSI value, the higher the susceptibility to flooding, and vice versa.

3.3.2. Analytical hierarchical process (AHP)

Spatial judgement troubles have been resolved using multi-criteria decision analysis (MCDA). MCDA offers a variety of methods and practices for systematizing decision difficulties like spatial uncertainty issues and planning decisions through evaluation criteria (Malczewski 2006). The analytical hierarchical process (AHP) is a multi-criteria assessment tool used for decision-making. The AHP deals with unstructured, complex and multiple-attribute issues and was first developed by Saaty (Saaty 1980). The AHP approach determines the weightings of multiple criteria through the in-depth knowledge and judgement of experts in the field (Saaty and Vargas 1984). A categorized order of factors or attributes and arithmetical values are established based on the significance of each criterion (Cabrera-Barona and Ghorbanzadeh 2018; Ghorbanzadeh et al. 2018b). The attributes are integrated, and each of these factors is given the weight according to its significance (Sahnoun et al. 2012). The AHP approach is used to generate the correlative pairwise comparison matrix that is created from the expert's opinion based on their in-depth knowledge about the prominence of each factor and comparing each of these factors with all the other factors. The expert allocates a value to each attribute. In the AHP process, the transitivity

Table 1. Pairwise comparison point-based rating scale of AHP.

Importance level	Ranking
Equally important	1
Equally important to slightly more important	2
Slightly more important	3
Slightly more important to much more important	4
Much more important	5
Much more important to very much more important	6
Very much more important	7
Very much more important to extremely important	8
Extremely important	9

principle is quite significant for any of the factors, like a1, a2, a3, for example. This can be defined as if a1 > a2 and a2 > a3, then a1 > a3. The principle of transitivity is maintained in the AHP process, where the weights/values are assigned to each attribute or conditioning factor. Owing to the principle of transitivity, a consistent pairwise comparison matrix would mean that if 2a1 > a2 (i.e. a1 is twice more desirable than a2) and 4a2 > a3, then 8a1 > a3 (Taha et al. 2019). Inconsistency is well-defined and based on the assumption that $\lambda max > n$ for comparison matrices and $\lambda max > n$, if C is a consistent comparison and the consistency ratio (CR) is defined by Equation (5):

$$CR = (\lambda max - n)/(RI(n-1) \tag{5}$$

Where RI is the random index of a randomly generated pairwise comparison matrix for $n = 2, 3, 4, 5, 6, 7, 8$, and 9. When the CR is <0.10, it signifies a suitable level of consistency, while a CR > 0.10 signifies a certain level of inconsistency (Saaty and Vargas 1984). Surveys were conducted to gather expert knowledge for the East Rapti basin to calculate the criteria weights using the AHP method. Each attribute is allocated a value based on the scale (Saaty and Vargas 1991) that ranges from zero to nine, and it is added to the matrix, as shown in Table 1.

3.3.3. Evidence belief function (EBF)

The Dempster–Shafer theory (DST) is a statistical method for identifying spatial integration based on a combination rule (Dempster 1967; Shafer 1976). DST is a spatial integration model that has a mathematical representation and is generally applied as a knowledge-based approach. The DST framework is used to estimate evidence belief functions (EBF) that are integrated based on the Dempster rule of combination (Dempster 1967). The EBF hypothesis determines the flood susceptibility of an area based on the given spatial evidence. The evidence belief functions are a composite of *bel* (degree of belief) (Equations (3) and (4)), *Dis* (degree of disbelief) (Equations (7) and (8)), *Unc* (degree of uncertainty) and *Pls* (degree of plausibility) in the range of 0 and 1. The following equations were used to run the EBF model.

$$\lambda(Tp) = N/D = [N(LIEij)/N(L)]/[N(Eij) - N(LIEij)/(N(A) - N(L)] \tag{6}$$

$$Bel = \lambda(Tp)Eij / \sum \lambda(Tp)Eij \quad (7)$$

(Tien Bui et al. 2019).

Where $N(LIEij)$ is the number of flood pixels in each class, $N(L)$ is the total number of floods, $N(Eij)$ is the number of pixels of each class, $N(A)$ is the total number of pixels, and N and D are the proportions of flood occurrence areas and non-flood areas, respectively (Tien Bui et al. 2019).

Similarly, Dis values were also obtained through Equations (9) and (10), as shown below:

$$\begin{aligned} \lambda(Tp)Eij &= K/H \\ &= [(N(L) - N(L\ Eij))/N(L)]/[N(A) - N(L) - N(Eij)/(N(A) - N(L)] \end{aligned} \quad (8)$$

$$Dis = \lambda(Tp)Eij / \sum \lambda(Tp)Eij \quad (9)$$

(Tien Bui et al. 2019).

Where K is the proportion of flooding that does not occur, and H is the proportion of non-flooding areas in other attributes outside the class (Tien Bui et al. 2019).

$$\text{Pls} - \text{Bel} = \text{Unc} \quad (10)$$

$$Dis = (1 - Pls) \quad (11)$$

$$Bel + Unc + Dis = 1 \quad (12)$$

(Tien Bui et al. 2019).

The lower and upper probabilities that evidence supports a hypothesis are represented by *Bel* and *Pls*. Hence, *Pls* is greater than or equivalent to *Bel*. *Unc* is equivalent to *Pls* − *Bel* and shows doubt (or ignorance) of one's belief in the hypothesis based on the given evidence (Equation (10)). If $Unc = 0$, then $Bel = Pls$. *Dis* is the belief that the hypothesis is untrue based on the evidence (Equation (11)); it is equal to 1 – *Pls* (Equation (8)). In the case that $Unc = 0$, then $Bel + Dis = 1$, as in the probability approach. Based on Dempster's rule of combination, *Bel, Dis*, and *Unc* are the EBFs used to integrate evidence. EBF has a unique benefit over other statistical approaches in that it evaluates the impact of each class of every flood conditioning factor and assesses the correlation amongst each factor and flooding.

3.3.4. Geons

Geons are well-defined by Lang et al. (2014) as 'geon (derived from Greek gē (Γῆ) = land, earth and the suffix -on = something being) is a type of region, semi-automatically delineated with expert knowledge incorporated, scaled and of uniform response to a phenomenon under space-related policy concern'. Geons are generally defined as spatial units that are homogenous in terms of varying space-time phenomena under policy concern (Gudiyangada Nachappa et al. 2020a)

A geon is a spatial object which is scale specific and has stability features like minimalized intrinsic variance and gradients towards the outside through the vector encoding (Hagenlocher et al. 2014; Lang et al. 2014). The geon method is a two-part process to achieve domain-specific (i.e. based on experts) and semi-automatic regionalization. In general, the geons approach, which generates composite objects (Tiede et al. 2010), is applied to the data in an analytic and taxonomical procedure followed by a sophisticated mapping scheme (Lang et al. 2014). Region-based image segmentation, which is a specific type of multicomponent regionalization, is applied, and results are generated based on spatial continuity and specific homogeneity criteria.

Multi-resolution segmentation (MRS) is a commonly used algorithm in object-based image analysis (OBIA) (Blaschke 2010). MRS creates homogenous image segments in a nested hierarchy of scaled representations. Spectral information is accumulated in a scale-adaptive manner, minimizing the loss of detailed information (Drăguţ et al. 2014). The goal of creating geons is to map policy-relevant spatial phenomena that have been validated by experts in an adaptive manner, and that are comparable to the corresponding scale of intervention. This helps us to envisage and understand the spatial distribution of various phenomena and thus enables us to better mitigate the adverse effects of flooding through planning and assessing intervention measures (Kienberger et al. 2009). All the conditioning factors were converted to 8 bit, have normalized values from 0 to 255, and are in GeoTIFF format. The segmentation processes and parameterizations were carried out in eCognition software. The normalization was done based on Equation (3):

$$\mathrm{Vi} = \frac{\mathrm{V} - \mathrm{Vmin}}{\mathrm{Vmax} - \mathrm{Vmin}} * 255 \tag{13}$$

(Kienberger et al. 2009)

Where Vi is the normalized value, V the causal factor value to be normalized, Vmin is the minimum value of the entire data range and Vmax the maximum value of the data range for the layer.

The multi-resolution segmentation (MRS) is a commonly used algorithm in OBIA for segmentation of an image into image objects (Baatz and Schäpe 2000). MRS begins at the pixel level and consecutively aggregates into objects of diverse shapes, sizes, and characteristics until it reaches a threshold of homogeneity, which is set by the user. The main concern in MRS is the selection of parameters, especially the scale parameter (SP). The Assessment of Scale Parameter tool (ESP) enables us to identify the ideal scales created on a local variance graph, by means of a single layer (Drăguţ et al. 2010). This approach was later extended into an automated tool (ESP2) for multiple layers (Drăguţ et al. 2014). The ESP2, which is executed in the eCognition Developer software, is an entirely automated method for selecting the scale parameters and delivers at three different scales using MRS. We used the ESP2 tool to obtain the optimal scale values, and the finest scale was used to generate the geons.

3.3.5. Receiver operating characteristics (ROC)

We used the receiver operating characteristics (ROC) approach to corroborate the six flood susceptibility maps obtained through the FR, AHP, EBF, FR geons, AHP geons,

and EBF geons using the validation data. The ROC method displays the assessment results in terms of the true positive rate (TPR) and the false positive rate (FPR) in the resulting flood susceptibility maps (Linden 2006; Ghorbanzadeh et al. 2018c; Chen and Li 2020; Lei et al. 2020b). Pixels that are correctly referred to as having a high susceptibility in the flood validation data are the TPRs, whereas the incorrectly labelled pixels are the FPRs. ROC curves are produced by plotting the TPRs against the FPRs. The area under the curve (AUC) is defined as the degree of accuracy of the resulting flood susceptibility maps (Wang et al. 2020; Chen et al. 2020a). The AUC indicates the possibility that more pixels were correctly labelled than incorrectly labelled. Greater AUC values signify a greater accuracy and lower AUC values signify lower accuracy of the susceptibility map. AUC values that are near to unity or 1 indicate a significant susceptibility map. An AUC value of 0.5 shows an insignificant map because it means the map was produced by chance (Baird et al. 2013).

4. Results

The flood susceptibility maps were derived using the per-pixel approaches of FR, AHP and EBF. Then, the weights from the per-pixel approaches were used for object-based aggregation using geons for FR, AHP and EBF. There is no standard technique for classifying the values in the susceptibility maps derived from various approaches. The resulting susceptibility maps were categorized into the five classes of very low, low, moderate, high and very high susceptibility using the quantile classification technique, which distributes the values into groups containing an equal number of values, rather than using the natural breaks classification in which values are aggregated or limited within some classes.

4.1. FR

The flood susceptibility maps were generated to identify the areas that are prone to flooding. The weights for FR and EBF was derived from the data, and the weights for AHP were obtained through expert judgement. The final weights for FR, AHP and EBF for the East Rapti are given in Table 2.

Figure 4 shows the flood susceptibility map created using the FR weighting approach and classified based on the quantile classification schema and categorized into the five classes of very low, low, moderate, high and very high flood susceptibility (Chen and Chen 2021). The flood susceptibility map derived from the FR method shows a very high susceptibility in the flow direction of the East Rapti river and in the central region of the basin, and very low susceptibility in the northeastern part of the basin and in the southern tip of the region, as seen in Figure 4.

4.2. AHP

The expert-based AHP pairwise comparison matrix is shown in Table 3 for each conditioning factor. This was used to derive the weights shown in Table 2, which were used to create the final susceptibility map based on the AHP method.

Table 2. The EBF coefficient for spatial factors and classes along with the predictor ratings (PR) based on degrees of spatial associations along with the FR, AHP weights for factor classes (Althuwaynee et al. 2012).

Factors and classes	Bel	Min	Max	[Max-Min]	PR	FR weights	AHP weights	CR
Elevation		0.00	0.76	0.75	5.16			0.033
143–400	0.76					6.20	0.46	
400–800	0.15					1.25	0.27	
800–1200	0.06					0.47	0.16	
1200–1600	0.03					0.26	0.07	
>1600	0.00					0.03	0.04	
Curvature		0.19	0.57	0.38	2.60			0.037
Concave (–32 to –0.3)	0.24					0.95	0.18	
Flat (0.3)	0.57					2.22	0.49	
Convex (0.0017 to 26)	0.19					0.74	0.33	
Slope		0.00	0.92	0.92	6.32			0.014
0–5	0.92					2.03	0.42	
05–12	0.06					0.13	0.27	
12–20	0.02					0.05	0.17	
20–28	0.00					0.00	0.09	
>28	0.00					0.00	0.05	
Distance from drainage		0.03	0.29	0.26	1.78			0.042
0–400	0.21					2.37	0.44	
400–800	0.29					3.16	0.3	
800–1200	0.25					2.76	0.15	
1200–1600	0.22					2.47	0.07	
>1600	0.03					0.29	0.04	
Landcover		0.00	0.58	0.58	4.01			0.045
Forest	0.030					0.48	0.36	
Snow/glacier	0.000					0.00	0.23	
Grassland	0.000					0.00	0.16	
Agricultural area	0.106					1.73	0.11	
Barren area	0.271					4.41	0.06	
Builtup area	0.010					0.16	0.04	
Waterbody	0.584					9.50	0.04	
TWI		0.06	0.46	0.40	2.77			0.017
<8	0.06					0.96	0.45	
8–10	0.11					1.81	0.31	
10–12	0.46					7.50	0.12	
12–14	0.08					1.31	0.07	
>14	0.29					4.65	0.05	
SPI		0.06	0.49	0.43	2.95			0.017
<–2	0.49					2.30	0.41	
–2–0.22	0.20					0.94	0.27	
–0.22–1.55	0.06					0.27	0.16	
1.55–4.15	0.06					0.31	0.1	
>4.15	0.19					0.91	0.06	
Flow direction		0.06	0.21	0.15	1.00			0.083
East	0.13					0.97	0.02	
South East	0.07					0.55	0.16	
South	0.15					1.11	0.09	
South West	0.11					0.84	0.14	
West	0.21					1.54	0.08	
North West	0.11					0.77	0.16	
North	0.15					1.11	0.14	
North East	0.06					0.47	0.21	

Figure 5 shows the flood susceptibility map derived through the AHP approach and categorized into five classes using the quantile classification schema. The flood susceptibility map derived through AHP displays more very high susceptibility zones in the western region and towards the central region whereas the low susceptibility areas are in the northeastern and southern parts of the region.

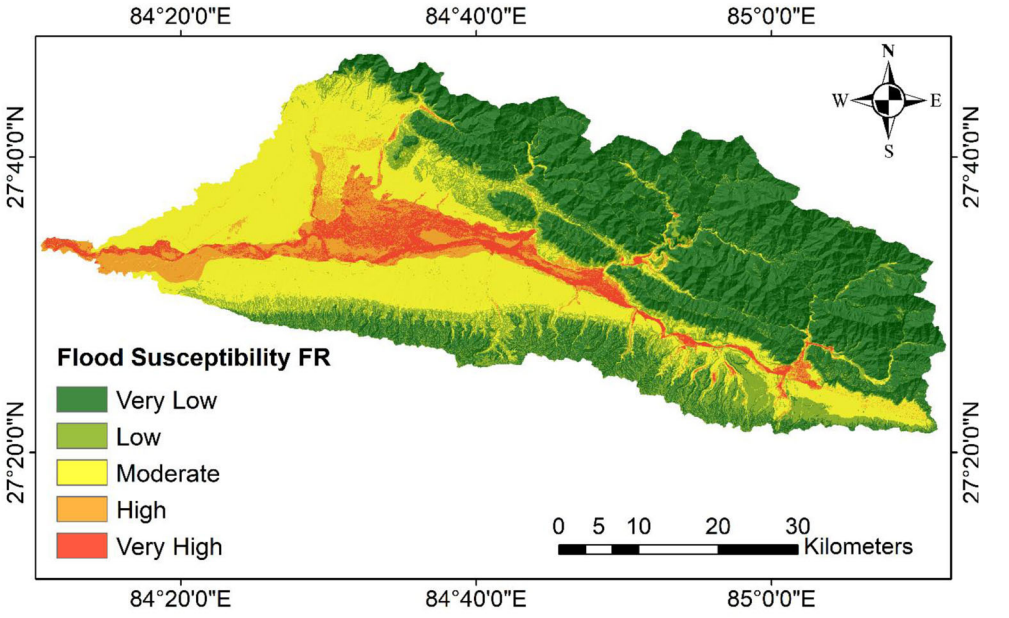

Figure 4. The flood susceptibility map derived from the FR approach for the East Rapti basin.

4.3. EBF

The flood susceptibility map based on the belief function of EBF is shown in Figure 6. The results are categorized into the five classes of very low, low, moderate, high, and very high flood susceptibility. The EBF-derived flood susceptibility map shows a similar pattern to the AHP-derived susceptibility map where the high-level susceptibility areas are located in the western region and towards the central region. In contrast, the low susceptibility areas are mainly in the northeastern region.

4.4. Ensemble using geons (per-pixel and object-based)

Weights from the per-pixel approaches of FR, AHP and EBF were used for the aggregation based on the object-based geon. The weights were used for segmentation to generate the flood susceptibility maps based on the object-based geon approach. The resulting flood susceptibility maps using the geon aggregation approach for East Rapti are shown in Figure 7 for the FR geons, in Figure 8 for the AHP geons, and in Figure 9 for the EBF geons. The resulting values in the maps were categorized based on the same quantile classification method as described above for the per-pixel approach. The ensemble approach of FR geons shows a more prominent very high susceptibility class in the proximity of the river compared to FR approach.

Although the AHP geons approach shows similar trends to the AHP approach, the high susceptibility class is more prominent compared to that in the AHP susceptibility map.

The EBF geons-based susceptibility map shows similar trends to that of the AHP geons, but the EBF geons map displays uniform susceptibility for all classes, which is quite different compared to all the other approaches.

Table 3. Pairwise comparison matrix and relative score of each parameter for the analytical hierarchy process (AHP) model.

	Elevation	Flow direction	Distance to drainage	Slope	SPI	TWI	Landcover	Curvature
Elevation	1	1/2	1/3	1/3	9	7	3	2
Flow direction	2	1	2	4	5	4	3	3
Distance to drainage	3	1/2	1	1/3	1/5	1/4	3	5
Slope	3	1/4	3	1	3	2	3	3
SPI	1/9	1/5	5	1/3	1	1/3	1/3	1/2
TWI	1/7	1/4	4	1/2	3	1	1	1/4
Landcover	1/3	1/3	1/3	1/3	3	1	1	1/4
Curvature	1/2	1/3	1/5	1/3	2	4	4	1

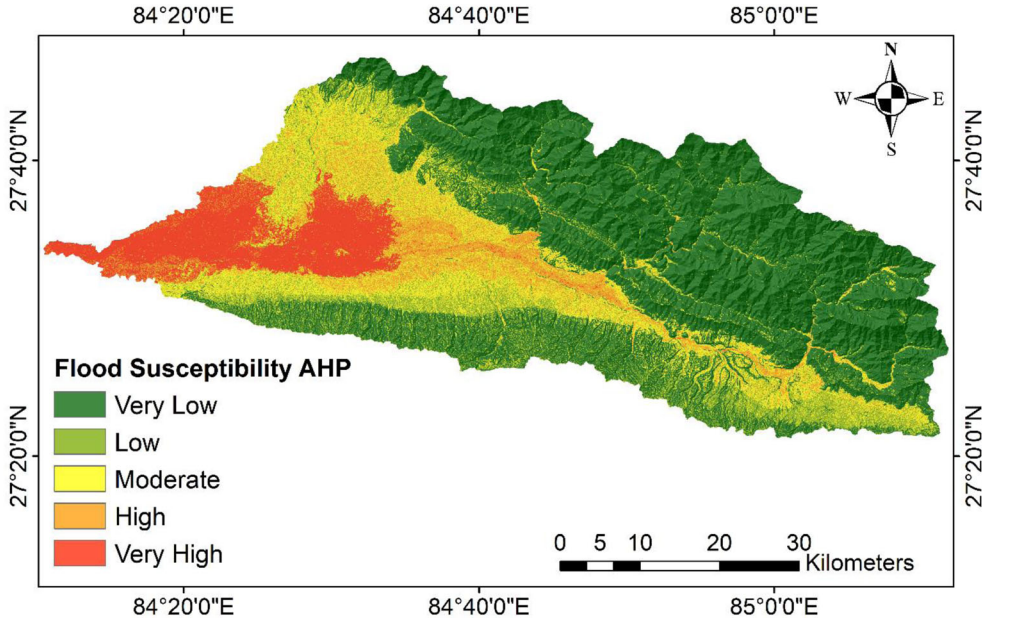

Figure 5. The flood susceptibility map derived from the AHP approach for the East Rapti basin.

Figures 7–9 show the regionalization from the object-based geon aggregation approach for FR, AHP and EBF, whereby all are devoid of administrative boundaries, and susceptibility classes are created based on the level of susceptibility.

It is crucial to understand how the ensemble of per-pixel and object-based approaches of FR geons, AHP geons and EBF geons flood susceptibility maps were derived and how each conditioning factor influences the susceptibility regions. The weightings from each approach influence the resulting map; however, it is uncertain how each location is affected by each conditioning factor. To demonstrate the impact of the conditioning factors, we chose one random location from each of the ensembled susceptibility maps derived using the geon approach and assessed the influence of each conditioning factor on the resulting susceptibility maps of FR geons, AHP geons and EBF geons. The randomly chosen susceptibility regions are shown in Figure 10.

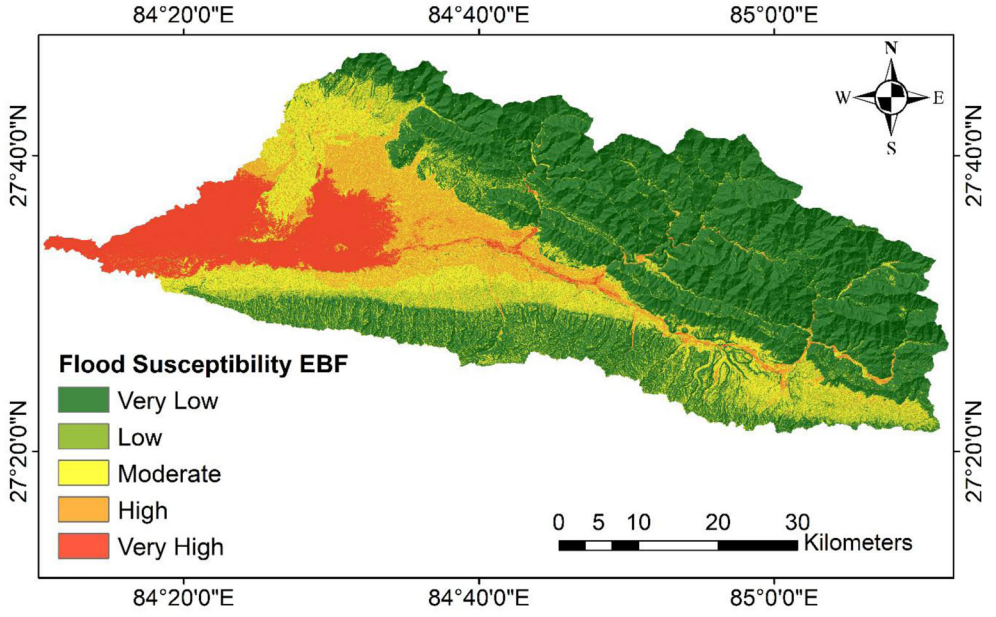

Figure 6. The flood susceptibility map derived from the EBF approach for the East Rapti basin.

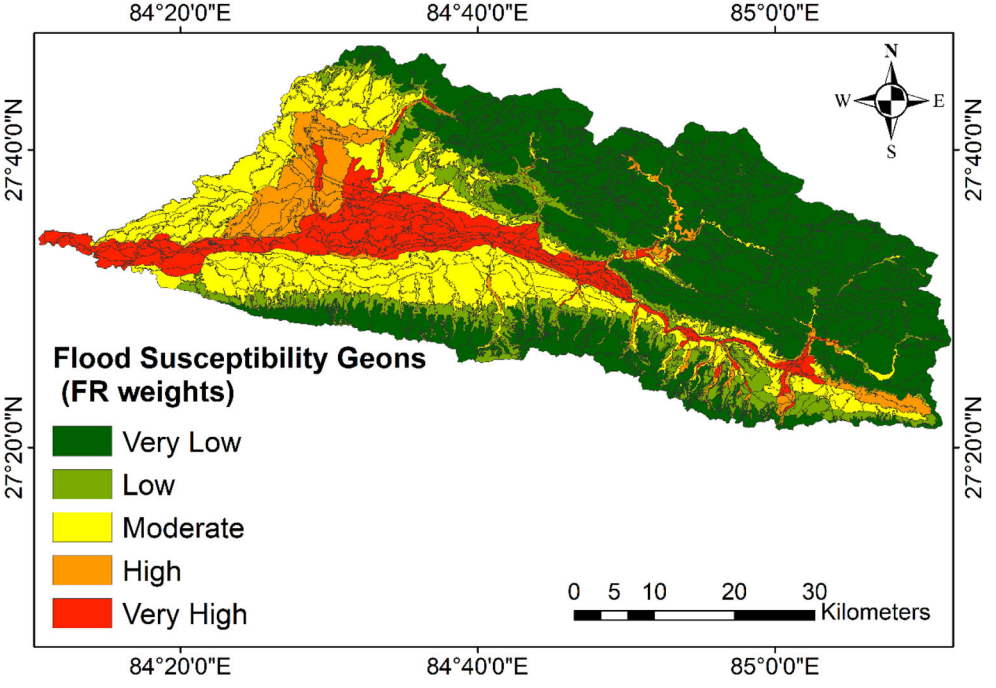

Figure 7. The flood susceptibility map derived from the FR geons approach for the East Rapti basin.

Figure 11 shows all the conditioning factors used to assess the impact of the selected conditioning factor. Each selected region from the geons ensemble approach of FR geons, AHP geons and EBF geons show the impact of each conditioning factor

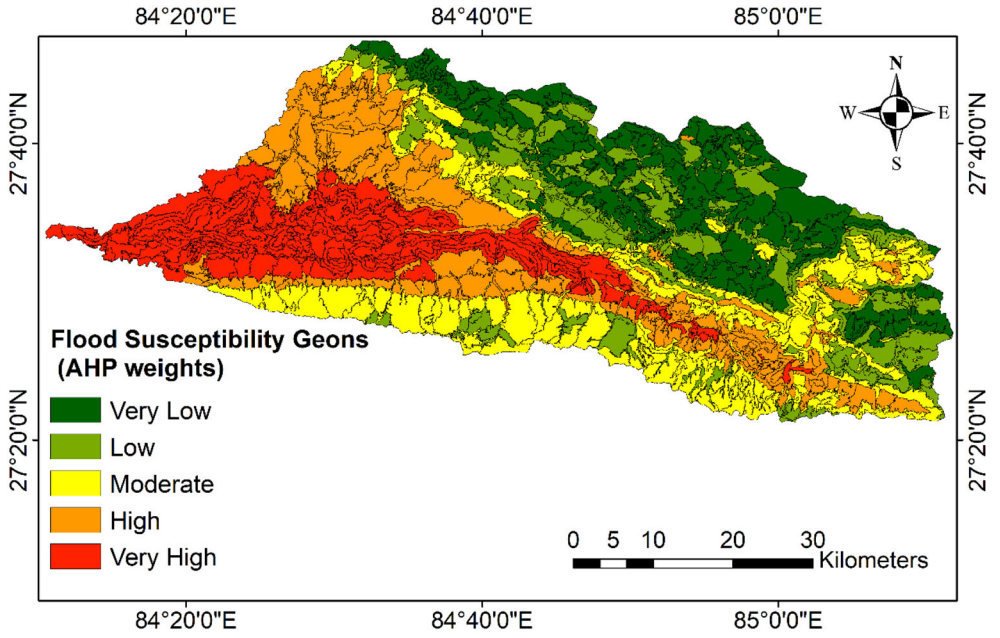

Figure 8. The flood susceptibility map derived from the AHP geons approach for the East Rapti basin.

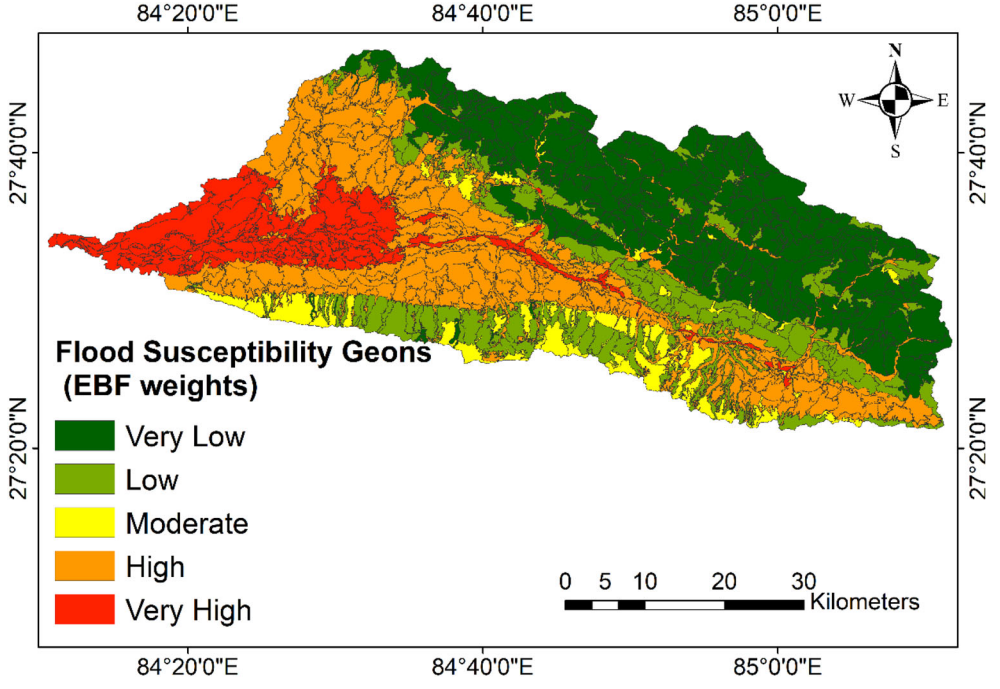

Figure 9. The flood susceptibility map derived from the EBF geons approach for the East Rapti basin.

compared with the different weights derived by the geons approach of FR, AHP and EBF to obtain the susceptibility class in each region.

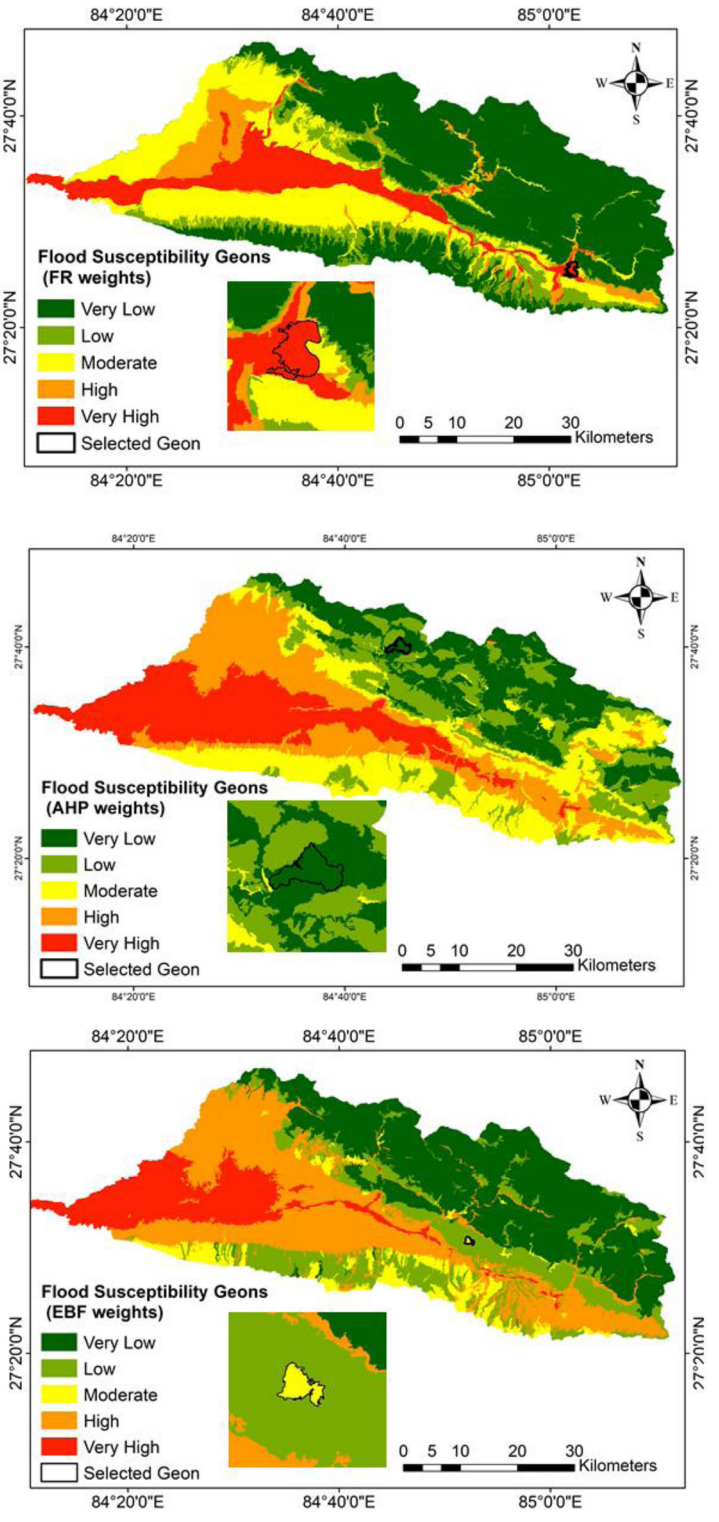

Figure 10. The random locations were chosen from the resulting maps of FR geons, AHP geons and EBF geons for impact assessment of conditioning factors.

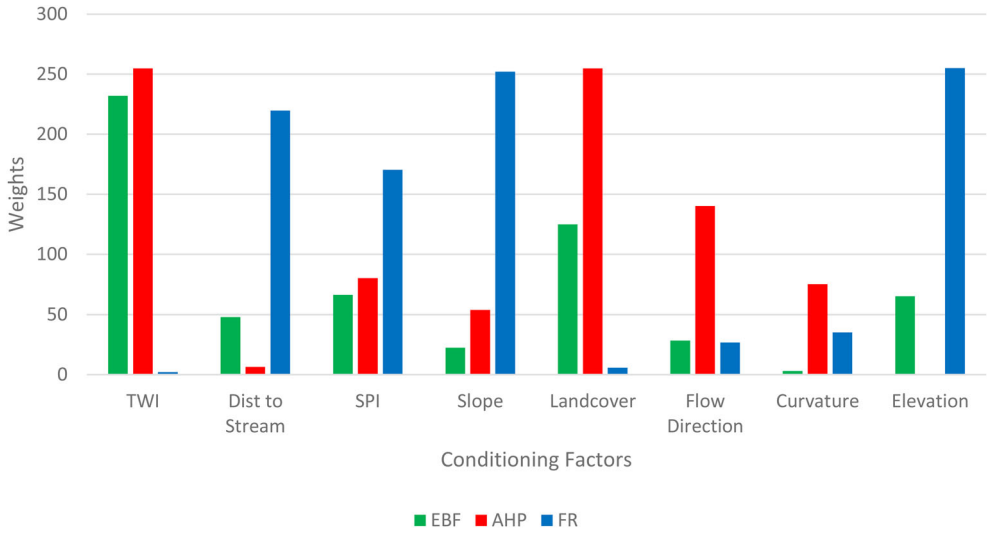

Figure 11. The impact of each input conditioning factor for the ensemble approach of FR geons, AHP geons and EBF geons for the East Rapti basin.

For the FR geons in the selected location, the elevation and slope have the highest impact in what is categorized as a very high susceptibility region, and the landcover and TWI have the least impact in the selected region. For the AHP geons, in what is categorized as a very low susceptibility region, the main impact is from TWI and landcover, whereas the distance to drainage has the least impact at the selected location. For the EBF geons, the selected susceptible region is categorized as moderate. The TWI has the most significant impact on flood susceptibility in this region, whereas the slope and flow direction have the least impact.

The impact of each conditioning factor varies for each susceptibility region and depends on the susceptibility categorization. This is quite important to know in order to understand the impact of each conditioning factor in determining the outcome of the flood susceptibility regions.

5. Validation

Validation is a vital phase in the process of producing natural hazard susceptibility maps for the benefit of planners (Ghorbanzadeh et al. 2018a). Different validation approaches determine the quality of the generated susceptibility maps. We compared the resulting maps from the per-pixel approach of FR, AHP, EBF with the per-pixel and object-based Geons ensemble approach with the flood inventory data. To estimate the efficiency of each model for flood susceptibility mapping, the conformity between the inventory data and the resulting maps indicated whether the applied models could correctly predict the areas that are susceptible to flooding (Pourghasemi and Rahmati 2018). There is no commonly adopted standard for allocating inventory data into training and validation data (Tsangaratos and Ilia 2016). However, in the literature concerning natural hazard assessment, the widely used split ratio for classifying the inventory data is 70/30, and we thus also used the same ratio for splitting

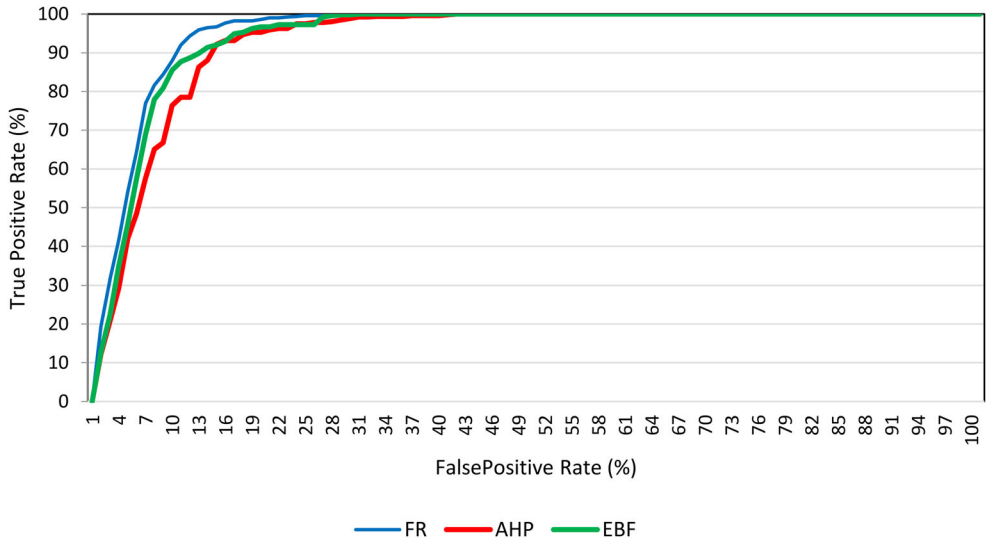

Figure 12. The ROC represents the quality method success rate curves for the per-pixel based FR, AHP and EBF approach for susceptibility mapping in the East Rapti Basin.

the available dataset into training and validations datasets (Li and Chen 2019). From the total flood locations, 30% of the flood locations were used to validate the results. In this study, we used the Receiver Operating Characteristics (ROC) approach to validate our results.

The accuracy values acquired from the ROC approach for the per-pixel approaches of FR, AHP and EBF are shown in Figure 12. The FR shows the most accurate results with an AUC value of 0.93, followed by the EBF with an AUC value of 0.92 and the AHP with an AUC value of 0.91. These results are excellent as they are close to unity or one, as displayed in Table 4 (Nachappa et al. 2020).

The data-driven FR, which is a simple yet widely used per-pixel approach, shows the highest AUC values compared to the expert-based AHP and belief function EBF. The results of the AHP might vary as this method is based on the expert weightings and thus on the knowledge of the experts, whereas the FR and EBF are derived from the data.

Figure 13 shows the AUC values for the ensemble geons approach of FR geons, AHP geons and EBF geons. This shows that the ensemble of FR geons has the highest accuracy of 0.96, and that the AHP and EBF have the same accuracy result of 0.94. The ROC results show that the FR has the highest accuracy of the per-pixel approaches as well as for the ensemble of FR geons, which is the most appropriate method for flood susceptibility mapping in the East Rapti basin in Nepal. This could vary between different geographical locations and may also be influenced by the selection of flood conditioning factors.

6. Discussion

The results reveal the possibilities of the use of the ensemble per-pixel and object-based aggregation concept of geons for flood susceptibility mapping. The main reason

Table 4. AUC interval values with description (Nachappa et al. 2020).

AUC values	Description
1 – 0.90	Excellent
0.90 – 0.80	Good
0.80 – 0.70	Fair
0.70 – 0.60	Poor
0.60 – 0.50	Fail

behind using object-based geons was to have susceptibility areas or entities that are free of any administrative boundaries. This reduces the prejudices from the false boundaries in the study area. Geons also aid the identification of place-specific implementation measures for planners and policymakers. This enables the transformation of continuous spatial information into discrete objects to oversee deviations according to various hazards in a specific area.

The ROC validation results show that the ensemble Geons approach yielded more accurate results compared to the per-pixel approaches. The FR approach was more accurate than the AHP and EBF models, even when using the ensemble geons approach. The data-driven FR approach is simple and easy to apply for deriving the weights. The FR approach enables us to determine relationships between a dependent variable and numerous independent variables in a discrete form.

Comparative studies are needed to evaluate the performance of models in the same conditions and make a fair judgement about their efficiencies (Goetz et al. 2015). Flood susceptibility mapping is critical for assessing flood-prone areas. The results can help to better manage and plan risk mitigation measures. In this study, we produced flood susceptibility maps for the East Rapti basin in Nepal based on a past flood inventory dataset held in the Regional database system by the International Centre for Integrated Mountain Development (ICIMOD). The results of the validation show that the geons approach can be applied for flood susceptibility mapping with the highest accuracy of 0.96, whereas the AHP yielded a lower accuracy of 0.90 in the per-pixel approach The validation results also demonstrated that object-based ensemble models are well suited for flood susceptibility mapping and can even lead to higher accuracies compared to pixel-based approaches. Geons represent meaningful units, and thus, are likely to be more suitable than per-pixel results for planning and mitigation measures. The principal idea of the geon approach is that the final susceptibility entities are independent of administrative units. It can, therefore, reduce the biases from false boundaries in the landscape.

There have been studies that focus on various methodologies and models for diverse regions, and the methods and structures vary considerably, which results in diverse outputs and has an impact on the performance of the selected model. Machine learning (ML) has been used for flood susceptibility mapping for various regions in recent times, which shows that the accuracy and performance are better than when using the traditional models (Rahmati et al. 2015a; Tehrany et al. 2015a). Multi-criteria decision analysis has also been used for flood susceptibility mapping, and this approach has also been shown to be suitable (Stefanidis and Stathis 2013), as has the ensemble approach of multi-criteria and machine learning for flood susceptibility (Gudiyangada Nachappa et al. 2020b). Future work would be to use the object-

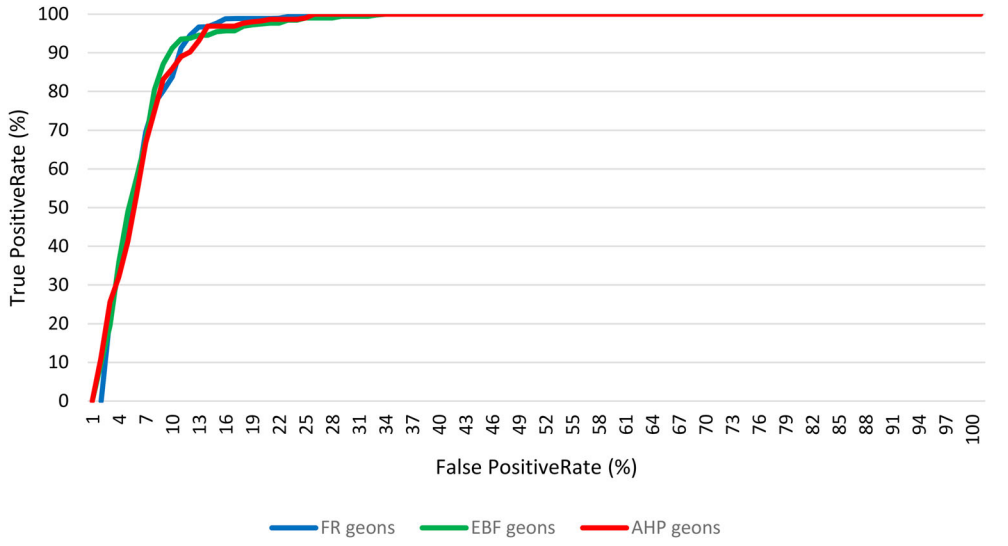

Figure 13. The ROC results show the quality method success rate curves for the ensemble of per-pixel and object-based FR geons, AHP geons, and EBF geons approach for susceptibility mapping in the East Rapti Basin.

based geons approach with machine learning models to check whether the accuracy is higher compared to the per-pixel approaches while having regions that are devoid of administrative boundaries. We would also like to apply this approach in a different geographical setting with different conditioning factors considered to be suitable for that particular region to compare and evaluate the model performance. It is crucial to control the conditioning factors for the hazard when preparing a natural hazard susceptibility map (Rahmati et al. 2015a). The performance of the selected model varies based on the selected conditioning factors, and, as we have more high resolution and greater conditioning factors, this might increase the performance and accuracy of the model. However, this all depends on the study area, along with the availability of the conditioning factors (Donati and Turrini 2002). Ensemble using Geons approach can be applied in a different physiographical region, like an alpine environment, to test the impact of the conditioning factors, which might vary and thus affect the approach used and its accuracy.

The regionalization from the object-based geons approach may be especially exciting and beneficial in defining the flood measures based on the highly susceptible regions rather than measures based on administrative boundaries. The geons approach can also be applied as part of the regional management principles to help mitigate the effects of flooding, reduce the socio-economic impact, and lessen the burden of the financial losses.

7. Conclusion

This research introduces the use of geons as an object-based aggregation approach for flood susceptibility mapping. The geons approach may also be applied to analyze the susceptibility of an area to other hazards. Future work will focus on using more

detailed historical flood event data and combine the object-based geon approach with sophisticated approaches like machine learning and deep learning to produce flood susceptibility maps. We would also like to assess various spatial resolutions of the source of the input data, i.e. the DEM, which might impact the results as well as the applied methodologies in various ways. The resultant susceptibility maps can be beneficial for local administration and civil protection entities to evaluate potentially affected areas in the cases of future floods. This study illustrates that geons can be applied to obtain meaningful susceptibility regions. This study may support spatial planners in decision-making and presents a strategic susceptibility mapping method that determines homogeneous landscape units and does not adhere to administrative boundaries. The results can be beneficial for planners and disaster management teams to identify the regions prone to floods and to mitigate the financial and economic damage caused by flooding in future.

Acknowledgements

The authors would like to thank Dr. Stefan Kienberger for his support and the anonymous reviewers for their constructive input.

ORCID

Thimmaiah Gudiyangada Nachappa http://orcid.org/0000-0002-1341-3264
Sansar Raj Meena http://orcid.org/0000-0001-6175-6491

Data availability statement

The data that support the findings of this study are available from the corresponding author, [S.R. Meena (sansarraj.meena@sbg.ac.at)], upon reasonable request.

Disclosure statement

No potential conflict of interest was reported by the authors.

References

Althuwaynee OF, Pradhan B, Lee S. 2012. Application of an evidential belief function model in landslide susceptibility mapping. Comput Geosci. 44:120–135.

Arabameri A, Rezaei K, Cerda A, Conoscenti C, Kalantari Z. 2019. A comparison of statistical methods and multi-criteria decision making to map flood hazard susceptibility in Northern Iran. Sci Total Environ. 660:443–458.

Baatz MM, Schäpe A. 2000. Multiresolution segmentation–an optimization approach for high quality multi-scale image segmentation. In: Angewandte Geographische Informationsverarbeitung XII: Beiträge zum AGIT-Symposium Salzburg, 5 to 7 July 2000, Salzburg, Austria.

Baird C, Healy T, Johnson K, Bogie A, Dankert EW and Scharenbroch C. 2013. A comparison of risk assessment instruments in juvenile justice. National Council on Crime and Delinquency.

Benz UC, Hofmann P, Willhauck G, Lingenfelder I, Heynen M. 2004. Multi-resolution, object-oriented fuzzy analysis of remote sensing data for GIS-ready information. ISPRS J Photogramm Remote Sens. 58(3–4):239–258.

Beven KJ, Kirkby MJ. 1979. A physically based, variable contributing area model of basin hydrology [Un modèle à base physique de zone d'appel variable de l'hydrologie du bassin versant]. Hydrol Sci J. 24(1):43–69.
Blaschke T. 2010. Object based image analysis for remote sensing ISPRS. J Photogramm Remote Sens. 65(1):2–16.
Blaschke T, Hay GJ, Kelly M, Lang S, Hofmann P, Addink E, Queiroz Feitosa R, van der Meer F, van der Werff H, van Coillie F, et al. 2014. Geographic object-based image analysis - towards a new paradigm. ISPRS J Photogramm Remote Sens. 87(100):180–191.
Cabrera-Barona P, Ghorbanzadeh O. 2018. Comparing classic and interval analytical hierarchy process methodologies for measuring area-level deprivation to analyze health inequalities. IJERPH. 15(1):140.
Chapi K, Singh VP, Shirzadi A, Shahabi H, Bui DT, Pham BT, Khosravi K. 2017. A novel hybrid artificial intelligence approach for flood susceptibility assessment. Environ Modell Softw. 95:229–245.
Chen W, Chen X, Peng J, Panahi M, Lee S. 2020a. Landslide susceptibility modeling based on ANFIS with teaching-learning-based optimization and Satin bowerbird optimizer. Geosci Front. 12(1):93–107.
Chen W, Li Y. 2020. GIS-based evaluation of landslide susceptibility using hybrid computational intelligence models. Catena. 195:104777.
Chen W, Zhao X, Tsangaratos P, Shahabi H, Ilia I, Xue W, Wang X, Ahmad BB. 2020b. Evaluating the usage of tree-based ensemble methods in groundwater spring potential mapping. J Hydrol. 583:124602.
Chen X, Chen W. 2021. GIS-based landslide susceptibility assessment using optimized hybrid machine learning methods. Catena. 196:104833.
Chowdhuri I, Pal SC, Chakrabortty R. 2020. Flood susceptibility mapping by ensemble evidential belief function and binomial logistic regression model on river basin of eastern India. Adv Space Res. 65(5):1466–1489.
Conforti M, Pascale S, Robustelli G, Sdao F. 2014. Evaluation of prediction capability of the artificial neural networks for mapping landslide susceptibility in the Turbolo River catchment (northern Calabria, Italy). Catena. 113:236–250.
Demir G, Aytekin M, Akgün A, İkizler SB, Tatar O. 2013. A comparison of landslide susceptibility mapping of the eastern part of the North Anatolian Fault Zone (Turkey) by likelihood-frequency ratio and analytic hierarchy process methods. Nat Hazards. 65(3): 1481–1506.
Dempster A. 1967. Upper and lower probabilities induced by a multivalued mapping. Ann Math Stat. 38(2):325–339.
Donati L, Turrini MC. 2002. An objective method to rank the importance of the factors predisposing to landslides with the GIS methodology: application to an area of the Apennines (Valnerina; Perugia, Italy). Eng Geol. 63(3–4):277–289.
Drăguţ L, Csillik O, Eisank C, Tiede D. 2014. Automated parameterisation for multi-scale image segmentation on multiple layers ISPRS. J Photogramm Remote Sens. 88(100): 119–127.
Drăguţ L, Tiede D, Levick SR. 2010. ESP: a tool to estimate scale parameter for multiresolution image segmentation of remotely sensed data. Int J Geogr Inform Sci. 24(6):859–871.
Felicísimo ÁM, Cuartero A, Remondo J, Quirós E. 2013. Mapping landslide susceptibility with logistic regression, multiple adaptive regression splines, classification and regression trees, and maximum entropy methods: a comparative study. Landslides. 10(2):175–189.
Ghorbanzadeh O, Blaschke T, Aryal J, Gholaminia K. 2018a. A new GIS-based technique using an adaptive neuro-fuzzy inference system for land subsidence susceptibility mapping. J Spatial Sci. 65(3):401–417.
Ghorbanzadeh O, Meena SR, Blaschke T, Aryal J. 2019. UAV-based slope failure detection using deep-learning convolutional neural networks. Remote Sens. 11(17):2046.

Ghorbanzadeh O, Moslem S, Blaschke T, Duleba S. 2018b. Sustainable urban transport planning considering different stakeholder groups by an interval-AHP decision support model. Sustainability. 11(1):9.

Ghorbanzadeh O, Rostamzadeh H, Blaschke T, Gholaminia K, Aryal J. 2018c. A new GIS-based data mining technique using an adaptive neuro-fuzzy inference system (ANFIS) and k-fold cross-validation approach for land subsidence susceptibility mapping. Nat Hazards. 94(2):497–517.

Glenn EP, Morino K, Nagler PL, Murray RS, Pearlstein S, Hultine KR. 2012. Roles of saltcedar (Tamarix spp.) and capillary rise in salinizing a non-flooding terrace on a flow-regulated desert river. J Arid Environ. 79:56–65.

Goetz J, Brenning A, Petschko H, Leopold P. 2015. Evaluating machine learning and statistical prediction techniques for landslide susceptibility modeling. Comput Geosci. 81:1–11.

Gokceoglu C, Sonmez H, Nefeslioglu HA, Duman TY, Can T. 2005. The 17 March 2005 Kuzulu landslide (Sivas, Turkey) and landslide-susceptibility map of its near vicinity. Eng Geol. 81(1):65–83.

Gudiyangada Nachappa T, Kienberger S, Meena SR, Hölbling D, Blaschke T. 2020a. Comparison and validation of per-pixel and object-based approaches for landslide susceptibility mapping geomatics. Nat Hazards Risk. 11:572–600.

Gudiyangada Nachappa T, Piralilou S, Gholamnia K, Ghorbanzadeh O, Rahmati O, Blaschke T. 2020b. Flood susceptibility mapping with machine learning, multi-criteria decision analysis and ensemble using Dempster Shafer Theory. J Hydrol. 590:125275.

Hagenlocher M, Kienberger S, Lang S, Blaschke T. 2014. Implications of spatial scales and reporting units for the spatial modelling of vulnerability to vector-borne diseases. GI_Forum. 2014:197.

Haghizadeh A, Siahkamari S, Haghiabi AH, Rahmati O. 2017. Forecasting flood-prone areas using Shannon's entropy model. J Earth Syst Sci. 126(3) : 39.

Hay GJ, Castilla G. 2008. Geographic Object-Based Image Analysis (GEOBIA): a new name for a new discipline. In: Blaschke T, Lang S, Hay GJ (Eds) Object-Based Image Analysis. Lecture Notes in Geoinformation and Cartography. Springer, Berlin, Heidelberg. https://doi.org/10.1007/978-3-540-77058-9_4

Hirabayashi Y, Mahendran R, Koirala S, Konoshima L, Yamazaki D, Watanabe S, Kim H, Kanae S. 2013. Global flood risk under climate change. Nat Clim Change. 3(9):816–821.

Hosseini FS, Choubin B, Mosavi A, Nabipour N, Shamshirband S, Darabi H, Haghighi AT. 2020. Flash-flood hazard assessment using ensembles and Bayesian-based machine learning models: application of the simulated annealing feature selection method. Sci Total Environ. 711:135161.

Jung IW, Chang H, Moradkhani H. 2011. Quantifying uncertainty in urban flooding analysis considering hydro-climatic projection and urban development effects. Hydrol Earth Syst Sci. 15(2):617–633.

Kargel J. 2016. Geomorphic and geologic controls of geohazards induced by Nepal's 2015. Gorkha Earthquake Sci. 351:aac8353.

Khosravi K, Nohani E, Maroufinia E, Pourghasemi HR. 2016. A GIS-based flood susceptibility assessment and its mapping in Iran: a comparison between frequency ratio and weights-of-evidence bivariate statistical models with multi-criteria decision-making technique. Nat Hazards. 83(2):947–987.

Khosravi K, Panahi M, Bui DT. 2018. Spatial prediction of groundwater spring potential mapping based on an adaptive neuro-fuzzy inference system and metaheuristic optimization. Hydrol Earth Syst Sci. 22(9):4771–4792.

Khosravi K, Shahabi H, Pham BT, Adamowski J, Shirzadi A, Pradhan B, Dou J, Ly H-B, Gróf G, Ho HL, et al. 2019. A comparative assessment of flood susceptibility modeling using multi-criteria decision-making analysis and machine learning methods. J Hydrol. 573: 311–323.

Kienberger S, Lang S, Zeil P. 2009. Spatial vulnerability units - expert-based spatial modelling of socio-economic vulnerability in the Salzach catchment. Nat Hazards Earth Syst Sci. 9(3): 767–778.

Kumar R, Anbalagan R. 2016. Landslide susceptibility mapping using analytical hierarchy process (AHP) in Tehri reservoir rim region, Uttarakhand. J Geol Soc India. 87(3):271–286.

Lang S, Kienberger S, Tiede D, Hagenlocher M, Pernkopf L. 2014. Geons – domain-specific regionalization of space. Cartogr Geogr Inform Sci. 41(3):214–226.

Lea Tien Tay MSA, Lateh H, Md KH, Kamil AA. 2014. Landslide hazard mapping of Penang Island using Poisson distribution with dominant factors. J Civil Eng Res 4: 72-77.

Lee S, Pradhan B. 2007. Landslide hazard mapping at Selangor, Malaysia using frequency ratio and logistic regression models. Landslides. 4(1):33–41.

Lei X, Chen W, Avand M, Janizadeh S, Kariminejad N, Shahabi H, Costache R, Shahabi H, Shirzadi A, Mosavi A. 2020a. GIS-based machine learning algorithms for gully erosion susceptibility mapping in a semi-arid region of Iran. Remote Sens. 12(15):2478.

Lei X, Chen W, Pham BT. 2020b. Performance evaluation of GIS-based artificial intelligence approaches for landslide susceptibility modeling and spatial patterns analysis ISPRS. IJGI. 9(7):443.

Levy J, Hartmann J, Li K, An Y, Asgary A. 2007. Multi-criteria decision support systems for flood hazard mitigation and emergency response in urban watersheds. J Am Water Resour Assoc. 43(2):346–358.

Li Y, Chen W. 2019. Landslide susceptibility evaluation using hybrid integration of evidential belief function and machine learning techniques. Water. 12(1):113.

Linden A. 2006. Measuring diagnostic and predictive accuracy in disease management: an introduction to receiver operating characteristic (ROC) analysis. J Eval Clin Pract. 12(2): 132–139.

Mahalingam R, Olsen MJ, O'Banion MS. 2016. Evaluation of landslide susceptibility mapping techniques using lidar-derived conditioning factors (Oregon case study) geomatics. Nat Hazards Risk. 7(6):1884–1907.

Malczewski J. 2006. GIS-based multicriteria decision analysis: a survey of the literature. Int J Geogr Inform Sci. 20(7):703–726.

Markantonis V, Meyer V, Lienhoop N. 2013. Evaluation of the environmental impacts of extreme floods in the Evros River basin using Contingent Valuation Method. Nat Hazards. 69(3):1535–1549.

Meena S, Ghorbanzadeh O, Blaschke T. 2019a. A comparative study of statistics-based landslide susceptibility models: a case study of the region affected by the Gorkha earthquake in Nepal. ISPRS Int J Geo-Inf. 8(2):94.

Meena S, Mishra B, Tavakkoli Piralilou S. 2019b. A hybrid spatial multi-criteria evaluation method for mapping landslide susceptible areas in Kullu Valley, Himalayas. Geosciences. 9(4):156.

Meena SR, Gudiyangada Nachappa T. 2019. Impact of spatial resolution of digital elevation model on landslide susceptibility mapping: a case study in Kullu Valley. Himalayas Geosci. 9:360.

Meena SR, Tavakkoli Piralilou S. 2019. Comparison of earthquake-triggered landslide inventories: a case study of the 2015 Gorkha earthquake. Nepal Geosci. 9:437.

Mohammadi A, Shahabi H, Bin Ahmad B. 2019. Land-cover change detection in a part of Cameron Highlands, Malaysia using ETM + satellite imagery and support vector machine (SVM) algorithm. Environ Asia. 12(2).

Mohammady M, Pourghasemi HR, Pradhan B. 2012. Landslide susceptibility mapping at Golestan Province, Iran: a comparison between frequency ratio, Dempster-Shafer, and weights-of-evidence models. J Asian Earth Sci. 61:221–236.

Moore ID, Grayson R, Ladson A. 1991. Digital terrain modelling: a review of hydrological, geomorphological, and biological applications. Hydrol Process. 5(1):3–30.

Mosavi A, Ozturk P, Chau K-w. 2018. Flood prediction using machine learning models: literature review. Water. 10(11):1536.

Nachappa TG, Ghorbanzadeh O, Gholamnia K, Blaschke T. 2020. Multi-hazard exposure mapping using machine learning for the state of Salzburg. Austria Remote Sens. 12(17):2757.
Nampak H, Pradhan B, Manap MA. 2014. Application of GIS based data driven evidential belief function model to predict groundwater potential zonation. J Hydrol. 513:283–300.
Oh H-J, Pradhan B. 2011. Application of a neuro-fuzzy model to landslide-susceptibility mapping for shallow landslides in a tropical hilly area. Comput Geosci. 37(9):1264–1276.
Pourghasemi H, Pradhan B, Gokceoglu C, Moezzi KD. 2013. A comparative assessment of prediction capabilities of Dempster-Shafer and weights-of-evidence models in landslide susceptibility mapping using. GIS Geomat Nat Hazards Risk. 4(2):93–118.
Pourghasemi HR, Rahmati O. 2018. Prediction of the landslide susceptibility: which algorithm, which precision? Catena. 162:177–192.
Pradhan B. 2009. Flood suceptible mapping and risk area delineation using logistic regression, GIS and remote sensing. J Spatial Hydrol. 9(2).
Pradhan B, Lee S, Mansor S, Buchroithner M, Jamaluddin N, Khujaimah Z. 2008. Utilization of optical remote sensing data and geographic information system tools for regional landslide hazard analysis by using binomial logistic regression model. J Appl Remote Sens. 2(1): 023542.
Rahmati O, Pourghasemi HR, Zeinivand H. 2015a. Flood susceptibility mapping using frequency ratio and weights-of-evidence models in the Golastan Province, Iran. Geocarto Int. 31(1):42–70.
Rahmati O, Zeinivand H, Besharat M. 2015b. Flood hazard zoning in Yasooj region, Iran, using GIS and multi-criteria decision analysis. Geomatics Nat Hazards Risk. 7(3):1000–1017.
Saaty TL. 1980. The analytic process: planning, priority setting, resources allocation. New York: McGraw.
Saaty TL, Vargas LG. 1984. Inconsistency and rank preservation. J Math Psychol. 28(2): 205–214.
Saaty TL, Vargas LG. 1991. Prediction, projection, and forecasting: applications of the analytic hierarchy process in economics, finance, politics, games, and sports. Boston, Kluwer Academic Publishers.
Sachdeva S, Bhatia T, Verma A. 2017. Flood susceptibility mapping using GIS-based support vector machine and particle swarm optimization: a case study in Uttarakhand (India). In: 2017 8th International Conference on Computing, Communication and Networking Technologies (ICCCNT)., Delhi, 2017, pp. 1-7, doi: 10.1109/ICCCNT.2017.8204182.
Sahnoun H, Serbaji MM, Karray B, Medhioub K. 2012. GIS and multi-criteria analysis to select potential sites of agro-industrial complex. Environ Earth Sci. 66(8):2477–2489.
Samanta S, Pal DK, Palsamanta B. 2018. Flood susceptibility analysis through remote sensing, GIS and frequency ratio model. Appl Water Sci. 8(2): 66.
Shafer G. 1976. A mathematical theory of evidence. Vol. 42. Princeton University Press, Princeton, New Jersey, United States.
Stefanidis S, Stathis D. 2013. Assessment of flood hazard based on natural and anthropogenic factors using analytic hierarchy process (AHP). Nat Hazards. 68(2):569–585.
Taha R, Dietrich J, Dehnhardt A, Hirschfeld J. 2019. Scaling effects in spatial multi-criteria decision aggregation in integrated river basin management. Water. 11(2):355.
Tehrany MS, Pradhan B, Jebur MN. 2013. Spatial prediction of flood susceptible areas using rule based decision tree (DT) and a novel ensemble bivariate and multivariate statistical models in GIS. J Hydrol. 504:69–79.
Tehrany MS, Pradhan B, Jebur MN. 2015a. Flood susceptibility analysis and its verification using a novel ensemble support vector machine and frequency ratio method. Stoch Environ Res Risk Assess. 29(4):1149–1165.
Tehrany MS, Pradhan B, Mansor S, Ahmad N. 2015b. Flood susceptibility assessment using GIS-based support vector machine model with different kernel types. Catena. 125:91–101.
Tiede D, Lang S, Albrecht F, Holbling D. 2010. Object-based class modeling for cadastre-constrained delineation of geo-objects. Photogramm Eng Remote Sens. 76(2):193–202.

Tien Bui D, Khosravi K, Shahabi H, Daggupati P, Adamowski JF, Melesse A, Thai Pham B, Pourghasemi HR, Mahmoudi M, Bahrami S, et al. 2019. Flood spatial modeling in Northern Iran using remote sensing and GIS: a comparison between evidential belief functions and its ensemble with a multivariate logistic regression model remote sensing. Remote Sens. 11(13): 1589.

Tsangaratos P, Ilia I. 2016. Comparison of a logistic regression and Naïve Bayes classifier in landslide susceptibility assessments: the influence of models complexity and training dataset size. Catena. 145:164–179.

Uddin K, Shrestha HL, Murthy MSR, Bajracharya B, Shrestha B, Gilani H, Pradhan S, Dangol B. 2015. Development of 2010 national land cover database for the Nepal. J Environ Manage. 148:82–90.

Van Westen C, Rengers N, Soeters R. 2003. Use of geomorphological information in indirect landslide susceptibility assessment. Nat Hazards. 30(3):399–419.

Wang G, Lei X, Chen W, Shahabi H, Shirzadi A. 2020. Hybrid computational intelligence methods for landslide susceptibility mapping. Symmetry. 12(3):325.

Wang Q, Li W. 2017. A GIS-based comparative evaluation of analytical hierarchy process and frequency ratio models for landslide susceptibility mapping. Phys Geogr. 38(4):318–337.

Wu Y, Li W, Wang Q, Liu Q, Yang D, Xing M, Pei Y, Yan S. 2016. Landslide susceptibility assessment using frequency ratio, statistical index and certainty factor models for the Gangu County. Arab J Geosci. 9(2): 84.

Youssef AM, Pradhan B, Hassan AM. 2011. Flash flood risk estimation along the St. Katherine road, southern Sinai, Egypt using GIS based morphometry and satellite imagery. Environ Earth Sci. 62(3):611–623.

Yu J, Qin X, Larsen O. 2013. Joint Monte Carlo and possibilistic simulation for flood damage assessment. Stoch Environ Res Risk Assess. 27(3):725–735.

Zhao X, Chen W. 2020. Optimization of computational intelligence models for landslide susceptibility evaluation. Remote Sens. 12(14):2180.